Instrumentation development for magneto-optical studies of thin films

Pavel Chvykov, University of Michigan

Adviser: Roy Clarke

Completed in compliance with the undergraduate honors physics thesis requirements

1. Background

People have been fascinated by magnetic properties of some materials for thousands of years. However, despite such a long history of investigation into the nature of magnetism, it was only within the last hundred years that a coherent picture of the origins of magnetic properties was drawn up. The reason for this being that many of the macroscopically observed effects and properties are rooted in purely quantum mechanical concepts. Hence, magnetism also provided great testing grounds for many fundamental concepts of quantum mechanics as it was developed. This new understanding of magnetic materials allowed for the development of much of the modern-day technology, including electronic information storage (e.g. hard drives, credit cards), magnetic sensors (e.g. MRI), and inductive circuits (e.g. transformers, electric motors, speakers, radio-transmitters, etc.).

However, this understanding is still far from complete, and experimental investigations in the field keep uncovering unexpected behaviors and phenomena. On the same note, the recent advances in the field now allow for the development of unprecedented technologies that could drastically improve the performance of existing devices or provide qualitatively new results. One major area that currently holds much promise is the study of thin film magnetic properties, which can be drastically different from those of bulk materials. What makes this area particularly exciting is that these magnetic properties can

be vastly enhanced and finely controlled by the method of the thin film preparation – film material, substrate and, deposition method all greatly affect the behavior of these films.

In this work, we have built a system for easy, fast and accurate measurements of hysteresis properties and magnetic anisotropy, and another for the observation of spin-waves in thin films under different conditions. These systems were then used to measure the properties of several different iron-gallium films, and the correspondence between the film structure and magnetic properties was observed. Fe-Ga samples are of particular practical interest due to the high coupling between magnetization and strain, and hence shape, observed in this material. Further, when used together, the hysteresis and spin-wave measuring systems can allow for novel comprehensive studies of correlations between the various magnetic properties and parameters in the films.

To begin, we must consider the origins of the basic magnetic properties observed in materials. Following is a qualitative description based on a more rigorous treatment presented in [1, 2, 3].

1.1 Magnetization

Perhaps the first question that people asked in connection with magnetism is why do different materials have different magnetic properties? Some can be observed to be “naturally” magnetic, others can be made to become and remain magnetic, others interact with magnetic materials, but do not retain magnetization, and yet others exhibit no magnetic properties at all. This distinction could only be fully explained with the development of quantum theory.

Magnetization (M) is defined as the magnetic dipole moment in the material per unit volume. All magnetic fields are originated by moving electric changes. In a solid, the charges present are the negative electrons and the positive nuclei, and thus, in the absence of currents, magnetic field is created

by the orbital angular momentum of the electron, and the electron and nuclear spins. For the case of simplest elemental magnetic materials, like Fe and Ni, it turns out that the most important contribution to the overall magnetic field is due to the electron spin. For other systems, like complex magnetic alloys, or isolated atoms, the spin and orbital contributions can have different strengths depending on the electronic structure of particular atoms and their environment. A descriptive picture of the magnetic materials relates to the Pauli Exclusion Principle, which forces the paired electrons that are sharing the same atomic or binding orbital to have opposite spins. In a consequent intuitive picture, we may explain the absence of magnetic properties in some materials based on the even cancelation of spin contributions, which results in a net zero magnetic moment of the material.

On the other hand, if the atoms in the material have unpaired electrons, and if the lattice spacing is close enough for these electrons' orbitals to overlap, then the spins of neighboring electrons couple via so-called Heisenberg exchange interaction. The two spins can be either parallel or anti-parallel, which, considering Pauli Exclusion, will result in two different spatial distributions of the orbitals. The two distributions will then have different Coulomb energies, hence causing either the parallel or anti-parallel state to be preferred. The parallel state forces the electrons to be in different energy levels, and if the lattice spacing is too small, causing the difference between the adjacent energy levels to be large, then this state has a higher energy, and is hence not preferred. Else, if the lattice spacing is too large so that the electron orbital overlap is small, then the corresponding exchange interaction is small, meaning that the spins of the unpaired electrons are uncoupled. In this case, an external magnetic field can align these spins, and hence create a net magnetic dipole in the material. However, as soon as the external field is removed, thermal affects will act to misalign them, and hence the individual electron magnetic moments cancel. This spin disorder leading to magnetic moment cancelation is known as paramagnetism.

Thus the exchange energy responsible for this interaction ($E_{ex}= -2J\mathbf{S}_i\cdot\mathbf{S}_j$) is proportional to the difference between the Coulomb energies of the two states. Due to the strict restrictions on lattice spacing described above, there are only a few materials (such as Fe, Co, Ni), called ferromagnetic, in which it is energetically favorable for the spins to align (J>0). In these materials, the energy balance (exchange interaction vs. thermal and other demagnetizing effects) will results in a spontaneous net magnetic moment when material is below a certain temperature known as the Curie temperature. Note that the classical magnetic dipole interaction between the spins of the electrons is much weaker than the exchange interaction, and cannot explain the observed magnetic properties. Also, the sensitivity of J to the lattice spacing allows drastically varying magnetic properties of the material by adjusting this spacing through the introduction of strain or dopants, which is somewhat more easily accomplished in thin films.

1.2 Magnetic anisotropy

It has been observed that in ferromagnetic materials, the spontaneous magnetization has preferred directions along which it occurs relative to the crystal lattice, sample geometry, etc. Similarly, the external magnetic field required to fully magnetize (saturate) such a material is found to be different along different directions. This indicates a spatial anisotropy in the magnetic properties of the material. The preferable direction of the magnetization (where the energy is lowest) is called the easy axis of the material, while the axis where the energy associated with such M orientation is highest is called the hard axis. The anisotropy of the material is measured by the anisotropy energy, which is defined as the difference between the energies needed to magnetize the material along its hard axis and its easy axis. There are generally four main causes of anisotropy.

The most important one, and the one studied in this work, is magnetocrystalline anisotropy (MCA), which is due to the anisotropic crystal lattice. Neither the exchange interaction nor the classical dipole coupling of the spins, neither of which couple with the anisotropic ordering of the crystal lattice, can account for this. Instead, MCA requires second order quantum perturbation theory. What is affected by the lattice most are the electron orbitals, which are deformed by the anisotropic electric fields present within the lattice. Hence, the orbital angular momentum couples to the lattice, while the electron spin couples to its orbit via magnetic dipole interaction. This indirect coupling of the spin to the lattice structure is referred to as pseudodipole and pseudoquadrupole couplings, due to the similarity of their form with regular dipole and quadrupole interactions. The direct spin-lattice dipole coupling is about 50 times weaker than this. Note that since natural materials are usually not monocrystalline, on average, this effect cancels.

A second origin for MCA is magnetoelastic anisotropy, which is due to strain forces in the film. Strains perturb the crystal lattice, changing lattice spacing anisotropically and hence, changing the MCA anisotropy. From considerations discussed in section 1.1, strain can also change the magnitude of the magnetization in ferromagnetic materials. Thus, both the direction and magnitude of magnetization couple to the strain in the lattice. As a result, a magnetic sample might be able to lower its magnetic energy by changing its shape slightly, and hence introducing strain. This is used in some applications to change the shape of material with applied magnetic fields, or conversely to change the magnetization by applying strain to the material.

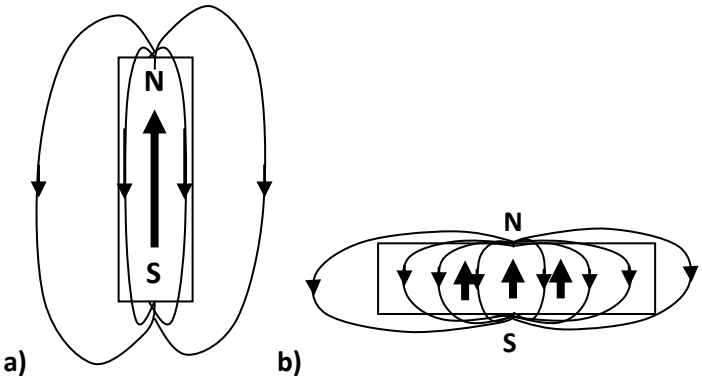

Fig. 1.1. Magnetostatic anisotropy: If magnetization of the two samples is the same, sample (b) produces a stronger magnetic field, which couples to the elementary dipoles, providing a stronger demagnetizing effect.

Another important source of anisotropy is magnetostatic, which is due to the shape of the sample of the material. If all the spins are aligned, then in the bulk of the material, any pole of an electron magnetic dipole will have an opposite pole nearby, and the two cancel each other when viewed macroscopically. At the surface however, the outside poles of the dipoles are unpaired, resulting in a net pole. This way, the sample becomes a familiar bar magnet. However, we must remember that the familiar field lines outside the magnet, from N to S pole, also pass through the magnet, and thus act to demagnetize it. For the two samples magnetized as shown in figure 1.1, the field produced by sample (b) is larger since the two poles are closer together and have a larger area with the same density of microscopic poles (if magnetization is the same for the two). Hence, the demagnetization field is larger for sample (b). In other words, (b) experiences a stronger magnetic coupling between the net dipole of the sample and the individual electron dipoles. So in general, it is harder to magnetize a sample along its short axis. This effect is particularly pronounced in thin films, where fields over 1.8 T are needed to produce magnetization normal to the plane of the film.

The final source of anisotropy is the surface anisotropy. This is caused by the inherently anisotropic environment of the surface atoms, as well as by the magnetostatic anisotropy across any imperfections on the surface (scratches, dents). This anisotropy, although only affects surface domains, can play an important role for magnetization reversal.

1.3 Domains

In section 1.1 we considered the strongest interaction that causes spins in ferromagnets to align. In section 1.2, we looked at the forces that cause these spins to align in certain preferred directions. These anisotropic forces are often uncorrelated with the exchange interaction, and it can happen that the interactions that cause anisotropy work against the exchange force that aligns the spins. Although the anisotropic interactions are weaker, they can act on larger scales. This balance results in the domain structure of ferromagnetic materials, where microscopically in any region the spins are all aligned, but there exist other similar regions with different directions of spin alignment. Such regions are called domains, and they typically range 5 – 100 μm in size in bulk materials.

The domain structure of the material is a result of the total energy minimization. The different factors that go into this minimization include contributions from the exchange interaction, magnetostatic energy, magnetocrystalline anisotropy, magnetoelastic anisotropy, as well as the Zeeman energy. The first three interactions in this list – exchange, magnetostatic and MCA – are always present and mostly determine the domain structure in unperturbed materials. The magnetostatic, or demagnetizing interaction is simply the classical magnetic coupling between all dipoles present, which tends to anti-align the spins. As mentioned before, for two adjacent electrons, this coupling is much weaker than the pseudodipole coupling given by the exchange force. However, the interaction between the net dipoles of two larger regions of aligned spins is strong enough to allow slight perturbations to the alignment of adjacent spins. These perturbations in relative orientations of the spins, while do not add much to the exchange energy, can add up to produce a 180^{o} rotation of the spin, and hence of the magnetic moment (Fig. 1.2a). This reversal of magnetic moment then lowers the magnetostatic energy in the material. As illustrated in figure 1.2b, when the domains are anti-aligned, there is less energy

stored in the magnetic field. In the third case in fig.1.2b, the magnetic circuit is closed, and hence the magnetostatic energy of the configuration is minimized at zeros, as is the net magnetic dipole moment. This third case also illustrates an important point about the domains near the boundaries of the material sample, which often tend to have a different orientation from the domains in the bulk.

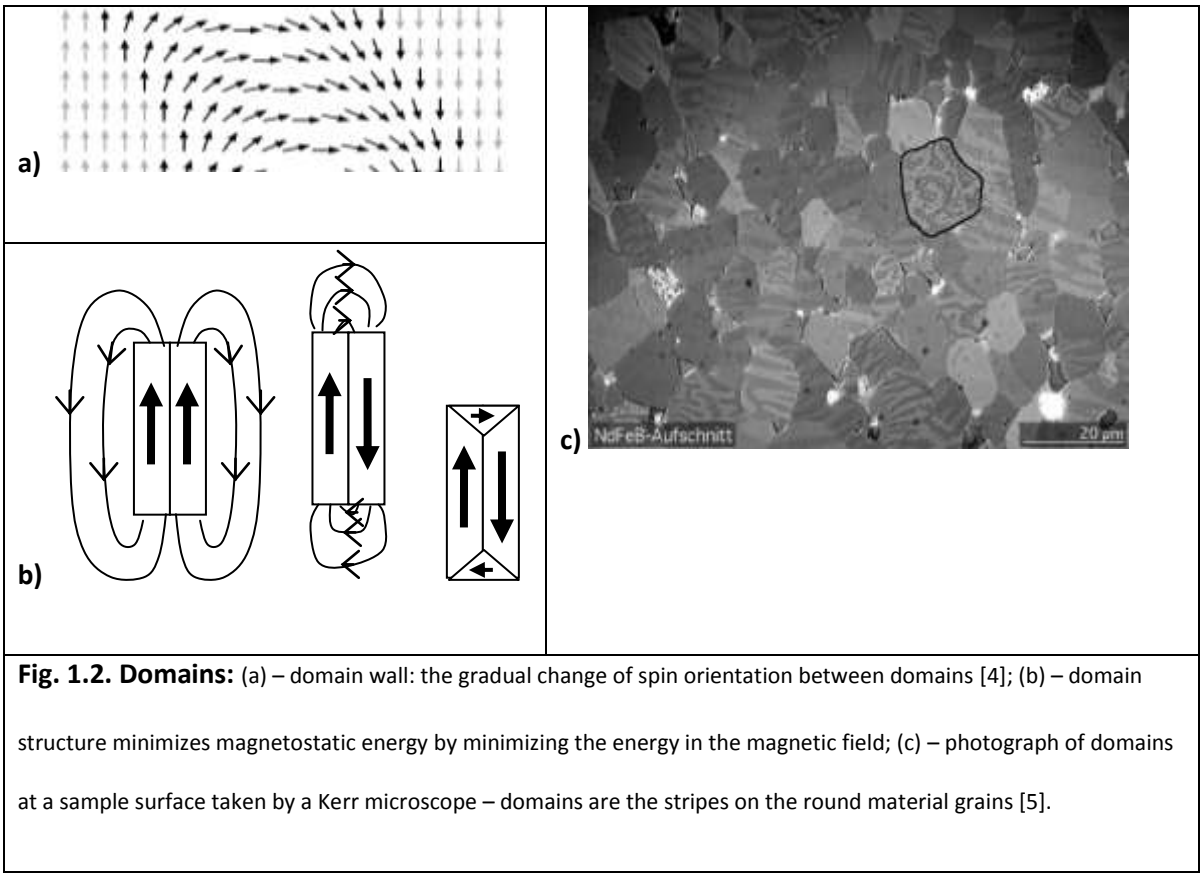

Fig. 1.2. Domains: (a) – domain wall: the gradual change of spin orientation between domains [4]; (b) – domain structure minimizes magnetostatic energy by minimizing the energy in the magnetic field; (c) – photograph of domains at a sample surface taken by a Kerr microscope – domains are the stripes on the round material grains [5].

There is one other important interaction which accounts for the observed discrete domain structure. If the exchange and magnetostatic interactions were the only participants in the domain formation, then the spin would gradually change throughout the sample, thus distributing the exchange energy increase over the whole sample. However, such a spin distribution would increase the MCA energy, and thus there is a potential driving the spins to align along the easy axes. This potential then accounts for the discrete domains that are observed in materials (fig.1.2c), and forces the domain walls (regions where spin is readjusting between the domains, fig.1.2a) to be narrow (~500 Å). Additionally,

minimization of the magnetostatic energy with the spins aligned along the easy axis accounts for the domains being elongated along the easy direction.

There can, of course, be other forces acting on the spins that further adjust the domain structure. One such contribution is due to the minimization of the wall energy. The existence of a domain wall is energetically costly due to the exchange interaction and the MCA energy, and hence, it is energetically favorable to minimize the domain wall length. Another example can be the magnetoelastic energy, which can adjust the MCA force, hence rotating the orientation of some domains. Finally, the Zeeman energy, which is simply the effect of an externally applied magnetic field, can of course be the determining interaction for large fields – at saturation, all domains in the material are aligned.

1.4 Hysteresis

At this point, we have the general picture for the static structure of magnetic materials. Now, we would like to discuss the dynamics of how this structure forms and changes under the influence of an external field. Such a field would upset the energy balance in the material by introducing the Zeeman energy term. Consider starting from an unmagnetized ferromagnetic material – due to the exchange interaction, the domains will still be present, but in general, they will be misaligned, thus cancelling the dipole moments. If we now apply a magnetic field, the domains experience a force rotating them towards the field orientation (fig.1.3a, going from 0 to A). When the field becomes strong enough, nearly all the domains are aligned, and the magnetization can no longer increase – thus the sample reaches saturation (fig.1.3a, point A). If we now reduce the field, still keeping it aligned in the same direction, anisotropic interactions will push the domains towards the easy orientation, if that is not already the case, balanced by the remaining external field and the potential barriers associated with any domain reorientation, explained below. Hence, when applied field is reduced to zero, or even reversed,

the direction of the net magnetization can be retained (point B). The remaining magnetization at this point is called the remanence. So a certain value of reverse field must be applied before magnetization drops back to zeros, this is the coercivity field (point C). If the reverse field is then increased further, domains align along it and saturation is reached once again. Hence, as we can see, the value of magnetization depends not only on the current magnetic field, but also on its history. The area enclosed by the loop is associated with the work done by the applied field to traverse it, and hence the energy dissipated.

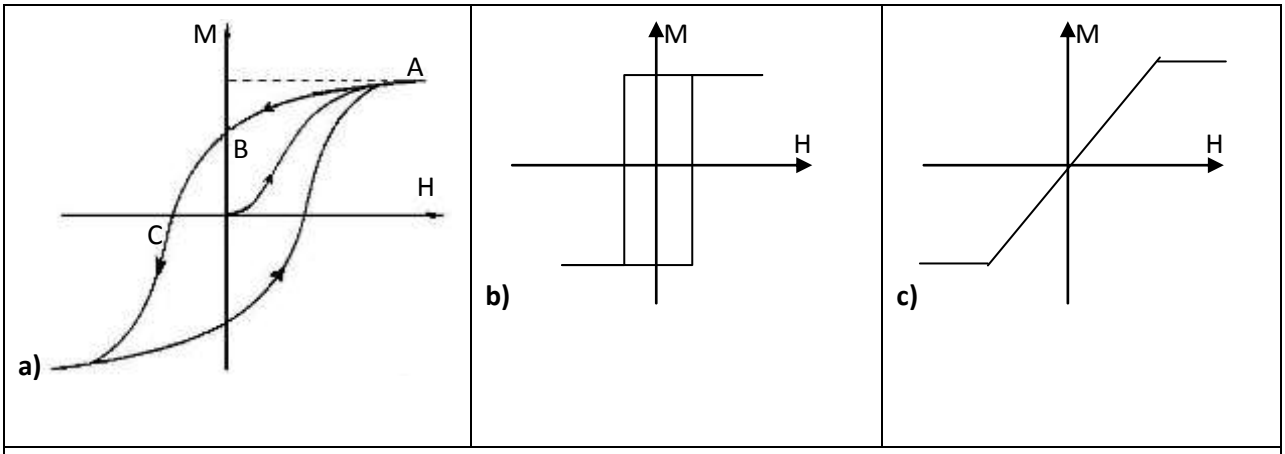

Fig. 1.3. Hysteresis: (a) – a typical hysteresis loop [6], (b, c) – hysteresis in a perfect monocrystal (uniaxial), applied field along the easy (b) and the hard (c) axis.

If the material sample studied is a perfect monocrystal, especially with uniaxial anisotropy (one easy, one hard axis, orthogonal to each other), then the loops will look more like figure 1.3b and 1.3c. If the applied field is along the easy axis (longitudinal loop - fig.1.3b), then as the field is decreased from saturation, MCA causes the domains to retain their orientation, opposed only by the demagnetization (magnetostatic) forces, which can be much weaker. Hence, domains remain aligned, and magnetization remains constant at saturation until the Zeeman energy of the reverse field shifts the balance to the other side enough to overcome the potential barrier of reorientation. Then all domains rapidly rotate and the sample quickly reaches saturation in the opposite direction. If the field is applied along the hard

axis however (transverse loop - fig.1.3c), then as soon as it is decreased from saturation, MCA causes domains to reorient towards the easy axis, while the magnetostatic coupling, aided by thermal energy, causes different domains to anti-align. Hence, as the field is reversed, magnetization decreases uniformly as the dipoles rotate through the easy axis and to the reverse saturation. This drastic difference in hysteresis can be used to study the anisotropy of materials.

1.5 Magnetization reversal

From the above description, it is clear that one crucial effect that affects hysteresis is the potential barrier associated with domain reversal. Domain reversal can proceed via three different pathways. First, and easiest, is by domain wall motion. As mentioned, the domain walls (fig.1.2a) have a certain energy associated with them, but this energy need not change much as they move. Further, recall that due to magnetostatic force, the domains near the edges of the sample are often reversed. Hence, when magnetization reverses, these domains can expand to cover the entire sample. In this pathway, the coercivity field depends mainly on the potential barriers that the domain walls move through. These are caused by spatial variations in the exchange energy (for example due to crystal lattice imperfections or stresses), spatial variations in anisotropy (similar reasons), magnetostatic energy (aligns walls along the direction of M), and change of wall length. The sum of these energies creates a complicated potential landscape in which the walls move, and as they settle in local minima, hysteresis results.

If there are no domains present that are already anti-aligned with the rest of the sample (such as far away from the boundaries for example), then a new domain must nucleate first. Such nucleation requires much more energy than wall motion, and hence is not common in most real bulk materials. This high energy requirement is caused by the fact that when a domain is nucleated, it is originally small, and

hence the reduction of magnetostatic and Zeeman energies is small compared to the increase in the exchange energy in the wall. This is much the same as bubble formation in liquids. The high potential barrier also means that after a domain finally nucleates, subsequent wall motion, and hence the reversal, proceeds very rapidly (fig.1.3b).

Finally, the third pathway is by domain rotation, as in the case in fig.1.3c. This does not happen however for situations such as that in fig.1.3b due to the potential barrier created by a higher MCA energy along the hard axis. One other effect that is common to any change in magnetization is the eddy current generated by the variations in the local fields. This current adds another factor to the energy dissipation.

1.6 Thin films

At this point, we have the general picture of the effects accounting for the properties and behavior of regular magnetic materials. Now, let us consider what we would expect for the magnetic properties of thin films. First, we must look at the film preparation techniques and their physical structure.

Although there are several techniques for thin film growth, one of the more common ones is the vapor deposition, which was used for preparing the samples measured here. In this method, a block of the film material is heated in an ultra-high vacuum chamber (~10^{-10} torr), causing atoms to evaporate from the surface. Since the number of particles inside the chamber is extremely small, scattering among particles becomes highly unlikely. In this situation, the evaporated atoms follow a straight path to the substrate, where they form into a crystal lattice together with the lattice of the substrate. In general the procedure is somewhat more complicated and includes the deposition of several layers of different

materials, such as the buffer layer, protective coating, etc.

There are many ways in which the properties of the film produced can be drastically varied. One of the most important such ways is by choosing the substrate. Glass, being amorphous, promotes disordered film growth, while monocrystalline substrates, such as MgO crystal, promote high ordering in the film lattice. Furthermore, lattice matching is an important consideration – the lattice spacing of the film material and the substrate need to geometrically match up in some way, otherwise the ordering of the film lattice on top of the substrate crystal becomes unfavorable. Furthermore, the orientation of the crystal lattice in the substrate will promote a certain orientation in the film lattice, thus qualitatively affecting anisotropy. Figure 1.4 shows and labels the three different orientations that a cubic lattice can adopt. Another way to affect film properties is to control the substrate temperature during deposition, thus controlling how ordered the film lattice is allowed to be. Applying a magnetic field during deposition or depositing at oblique incidence can create a uniaxial MCA. There are also many other control methods that are used.

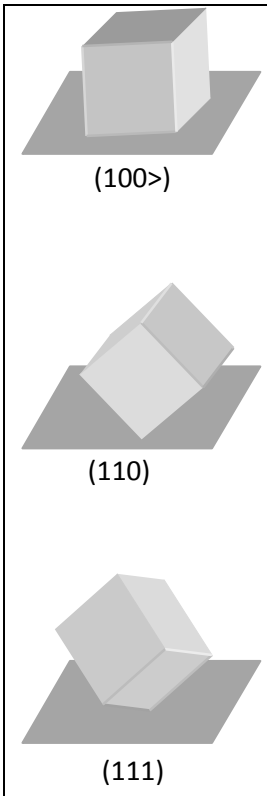

Fig. 1.4. Lattice orientations: the label gives the coordinates of one of the corners

The result is a thin film of ferromagnetic material on a non-magnetic substrate. The films can be from monolayers to microns in thickness (tens of monolayers is typical). The magnetic properties of these are then somewhat different from those of bulk materials. Firstly, the shape anisotropy is very strong here, and thus for the most part, the magnetization lies in the plane of the film. This effectively creates a two-dimensional problem, with important consequences. Recall that the domain structure is determined by the balance of the magnetostatic demagnetization, exchange energy in the walls and MCA. Hence, in this two-dimensional case, the wall area becomes much smaller, since it no longer has to

cover the entire surface of the domain. This then significantly reduces the contribution of the exchange energy in this energy balance, which then allows for more stable and much larger domains (100 μm – 1mm). Furthermore, the matching of the film lattice to that of the substrate, which in turn is near-perfect, allows to attain highly ordered and regular structure of the film lattice, and hence generally a more predictable and dramatic behavior. One other effect to consider is the stress in the film that results from imperfect lattice matching to the substrate. A similar stress results from heating the sample if the expansion coefficients of the film and the substrate are not matched. This stress results in additional magnetoelastic anisotropy.

Finally, due to the large domains and near-perfect lattice in these films, the hysteresis loops look more similar to the ideal cases in figures 1.3b and 1.3c. Due to the two-dimensional geometry, wall motion is more restricted, and hence is more difficult (less phase-space to move through) and takes longer, thus making nucleation more common than in bulk materials. The actual balance of the reversal mechanisms depends on the exact material and film structure. [7]

1.7 Magneto-Optic Kerr Effect

Magneto-Optic Kerr Effect (MOKE) is a very powerful experimental technique that was used in this work. In short, it is the reflection equivalent of Faraday effect –polarization rotation of the reflected light based on the magnetization of the reflector (rotation of order 0.1^{o}). Because the skin-depth of light in metallic materials is ~150 Å, this technique is especially sensitive to surface effects and so is ideally suited for thin films, while ineffective for detecting magnetization in bulk materials.

More precisely, the effect can be modeled by assuming different propagation speeds and different reflection coefficients for the two circular polarizations of incident light. The birefringence then

causes polarization rotation, while reflectivity difference creates polarization ellipticity. The effect can be explained from the simple consideration of Maxwell's equations. However to match the experiments, enormous magnetic fields (~1000 T) are required inside the sample. It turns out that this apparent internal magnetic field comes from the quantum mechanical spin-orbit coupling. Qualitatively, the polarization rotation results from spin-orbit interaction of the electron during the absorption and reemission of the circularly polarized photons being reflected. More precisely, the key to the polarization rotation is in the off-diagonal components of the complex conductivity tensor $\underline{\boldsymbol{\sigma}}$ in Ohm's law $\mathbf{J}=\underline{\boldsymbol{\sigma}}\mathbf{E}$, where **J** is the current density and **E** is the electric field. This tensor can be found by expressing the current as a probability current in QM, using the eigenstates of the electron Hamiltonian that includes spin-orbit interaction. This tensor then gives different indices of refraction for the two circular polarizations of incident light, and the Fresnel equations then give the exact reflection parameters.

Either way, the analysis is simpler if we consider the different off-diagonal components of the conductivity tensor separately – thus we consider three different geometries of the problem (fig.1.5). Generally, the coupling of the reflected photons to magnetization depends on the relative orientation of the electron and photon spins. In the polar geometry, the magnetization is normal to the surface, and effect is maximized at normal incidence of light. In longitudinal configuration, the magnetization is parallel to the sample surface and to the plane of incidence. Here, the effect is larger at oblique incidence, and vanishes at normal incidence. These two geometries are physically very similar – in both cases, the photon and electron spins couple when they are parallel, resulting in rotated elliptical polarization as discussed above. Further, for any orientation of the incident linear polarization, the

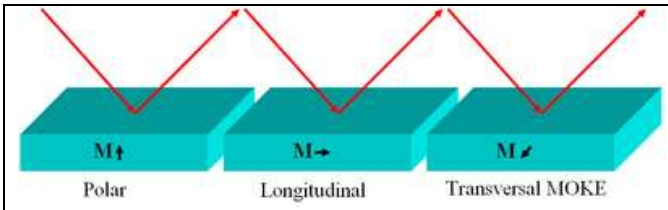

Fig.1.5. Kerr effect: The three components of magnetization affect the reflected light in different ways [8].

effect will be the same since the two circularly polarized components are affected. Finally, these effects are linear with the corresponding components of magnetization. In the case of transverse MOKE, when the magnetization is parallel to the surface, but perpendicular to the plane of incidence, the situation is very different. Since the magnetization is orthogonal to the photon spin, the physical mechanisms are somewhat different. Here, only the reflectivity coefficient for linearly p-polarized light is affected by magnetization, and no polarization rotation is observed. As for longitudinal MOKE, this effect vanishes at normal incidence. The small change in reflectivity in this effect is also more difficult to detect than the polarization change in the other two cases due to the large background, and hence this effect is used more sparingly. Due to these differences in behavior, the three magnetization components can be individually measured by choosing the right geometry and adjusting the incident polarization along with the analyzer (see also Chapter 2). There is also a higher order Kerr effect that is present in some materials which depends on the combinations of the different components, and is hence more difficult to separate out.

In this work, longitudinal MOKE geometry was used with s-polarized incidence, and polarization rotation was measured by detecting the intensity after passing the reflected light through a polarizing analyzer. [9]

1.8 Spin-waves

One curious phenomenon that occurs in magnetic materials is spin-waves. Just as phonons are propagating perturbations in the position of the atoms in the crystal lattice, in a similar way spin-waves (or magnons) are propagating perturbations of the orientation of the spins. Most any transient perturbation to the material, such as that of heat, strain, or applied field, can excite a magnon by

perturbing the orientation of some of the spins. After the perturbing interaction is removed, spins settle back to their instantaneous lowest energy state, and begin to oscillate in their energy wells or, more realistically, precess about the axis of lowest magnetic energy. The exchange interaction then couples these oscillations to the spins of adjacent electrons, thus causing the perturbation to propagate. However, there is one qualitative difference between the propagation of magnons and phonons. This is due to the fact that besides the exchange interaction, spins are also affected by magnetostatic coupling. As mentioned before, these two forces generally oppose each other, but act on different length scales. On larger scales, the magnetostatic interaction can counteract the exchange force and dominate the spin wave properties since the exchange energy is relaxed through alignment of the spins. In this case, because the exchange force is what drives the wave propagation, the observed spin waves characterized by a large wavelength propagate slower. Hence unlike phonons, where speed depends only on material parameters, spin-waves are governed by a non-linear dispersion relation (fig. 1.6). The result is the existence of different dynamic modes of the spin-precession. If the original perturbation affects a large region of the material, then within that region, spins will precess uniformly (parallel) together, and the region remains mostly stable, whereas for microscopic initial perturbations, magnons can travel at speeds of order km/s or more. This can, for example, produce standing waves within the thickness of the film.

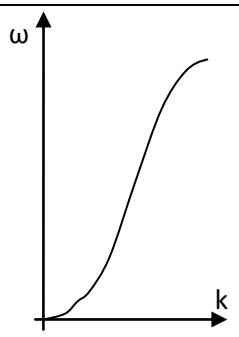

Fig.1.6. Spin-wave dispersion relation

Spin-waves also look different for different existing magnetizations in the material due to the difference in the shape of the energy wells in which they oscillate. Further, since the exchange interaction is correlated with lattice spacing, magnons can couple to phonons, and hence dissipate on the scale of 10-1000 ps. All these effects can be measured by looking at the waveforms using the MOKE techniques described in section 1.7. Their frequency, amplitude and dissipation time at different

magnetizations can provide valuable information about the magnetic properties of the material, such as the gyromagnetic ratio, exchange constant, anisotropy energy, and the correlation between the exchange interaction and lattice spacing.

1.9 Applications

In today's world, magnetic materials are extensively used everywhere in our everyday lives, from computers to household appliances. Now, the nee improvements in our understanding of magnetism promise a very bright future of technological development in the field. One fascinating area of applications is with spintronics, where electron spin is used for control, detection and storage. One example of a simple device that uses this is the spin-valve. It is composed of two ferromagnetic films with a non-ferromagnetic metal in-between. When the two magnetizations are parallel, the electrons can freely transfer between the ferromagnetic layers because the available density of states is high. However, when the two ferromagnets are anti-parallel, then electrons require a much higher energy to pass, and so the valve is closed. Such valve can be used for example for detection of magnetic fields in magnetic memory applications. Another interesting application to information storage is the so-called racetrack memory. This essentially operates the same as a cassette with a magnetic film, but instead of accessing the information by mechanical motion, the magnetic bits are propelled along a ferromagnetic wire via domain wall propagation. [10]

Furthermore, there are also many applications of the various couplings between the magnetic and other forms of energy (magneto-elastic, magneto-optical, magneto-electric, magneto-thermal, etc.) In this work in particular, the properties of iron-gallium samples are studied due to their abnormally high magneto-elastic coupling coefficients [11]. Such materials can change their shape upon a change of magnetization, or vice versa. This can then be used for example in remote manipulation of microscopic

objects, thus opening perspectives for nanotechnologies. Magnetoelastic materials also have important applications in information storage. If we consider the information stored using the magnetization of some material, then we want to find a way to be able to easily change this magnetization, without introducing extra devices, such as electromagnets or coils. Thus, it would be useful to be able to change the magnetization simply by applying a potential difference across the storing particle. Hence, electro-magnetic coupling is required. One way to accomplish this is through magneto-elastic. If a voltage is applied, the dissipated power heats up the sample, which can then create stresses in it, which then couple to magnetization via magnetoelastic coefficients. Specifically, these stresses can change the anisotropy of the material, causing a domain to rotate over a potential barrier, and hence to subsequently remain on the other side. There are also many other very creative applications of magnetic materials, spin currents, and magnetic thin films, and so a solid theoretical understanding of the magnetic processes occurring in different materials and of their origins is necessary to isolate and amplify the desired effects.

2. Hysteresis measurements

The first part of this work focused on developing an improved setup for hysteresis measurements in thin films using magneto-optic Kerr effect (MOKE). The goal was to study hysteresis behavior and magnetocrystalline anisotropy (MCA) in Fe-Ga samples. Due to the high magnetoelastic coupling coefficients in these samples (magnetization coupling to strain, and hence to shape), they have much practical interest for many applications. Three Fe-Ga films and one Fe film reference were measured and their properties correlated to their physical structure. The experimental setup allowed a clear, high-resolution, real-time observation of hysteresis dynamics, revealing some peculiar behaviors during magnetization reversal.

2.1 Experimental setup

The experimental setup used for the MOKE measurements was in essence fairly simple (fig. 2.1a). Light from a 15 mW Helium-Neon laser is vertically polarized, reflected from the sample at ~20° incidence, and after passing through the polarizing analyzer set at near-extinction, collected by a photodiode. The external magnetic field is applied to the sample by an electromagnet along the surface of the film and the plane of incidence. In this configuration, the polar magnetization component is near zero due to shape anisotropy and the direction of the applied field. The transverse component is also small in this experimental arrangement, and since the incident light is s-polarized, the measurements shown here are not sensitive to the transverse MOKE. Thus, this configuration measures mainly the longitudinal MOKE (see fig.1.5) and can be also be sensitive to some small remnants resulting from a second order MOKE as we shall see in the following. The sample is mounted on a motorized rotation stage, with 0.01° angular step size to allow measurement of anisotropy. Finally a Gauss probe is placed near the sample surface to measure exact value of the applied magnetic field.

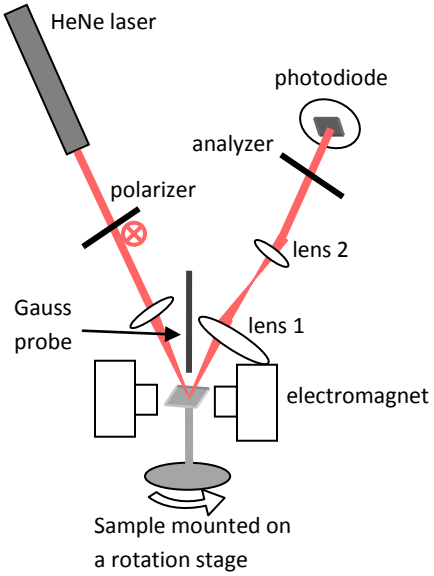

a)

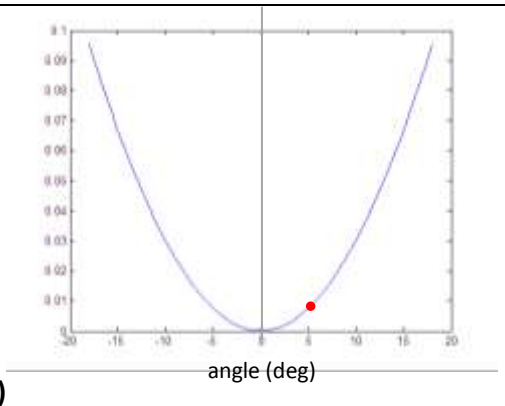

b)

Fig.2.1. Experimental Setup top vie; (b) – analyzer transmission function. The point marks that position used.

One important consideration is the analyzer orientation. The intensity transmission for the analyzer with respect to the incident polarization is a $\sin^2$ curve (fig.2.1b). To maximize the intensity variation that results for from a small change of angle (here $\Delta\theta \sim 0.1^o$), we want to maximize the derivative of the transmission function. However, this would occur at 45^o, and hence would result in a very large constant background signal, thus decreasing the sensitivity of the photodiode. Due to the balance between these two effects, a good setting for the analyzer angle at $\sim 5^o$ from extinction. Note that this is a large enough angle so that variations of $\pm 0.1^0$ are small enough so that the intensity varies linearly with the angle, and hence with magnetization.

The system of three lenses shown in figure 2.1 focuses the beam on the sample, but mainly serves the purpose of beam stabilization. The focusing itself does not affect the magnitude of the MOKE, and in our case was not tight enough to measure single domain magnetization. Hence, the magnetization measured was an average over several domains. However, the lens system nearly cancels the wobble of the reflected beam during sample rotation as shown in fig.2.1 (lens 2 is much closer to the focal position than lens 1). Due to geometry restrictions, it is impossible to control the angle of the sample without changing its position relative to the axis of rotation. The lenses lift the requirements on the mounting angle precision, thus allowing adjusting the sample position, which is necessary for small samples for example.

2.2 Measurement procedures

The measurement is also generally straightforward. The electromagnet is driven by a power-supply, which is in turn controlled by a signal generator, which outputs a sinusoidal driving signal. Thus, the Gauss-probe near the sample picks up the sine field that is produced. The signal from the photodiode is directly amplified and both signals are fed to a data acquisition module connected to a

computer. LabVIEW code is then used to analyze the data as soon as it is acquired (fig.2.2). The code triggers on the Gauss probe signal, averages over the set number of traces and plots the hysteresis loop. It then measures various parameters of the loop, including coercivity, remanence, saturation field, loop asymmetry, and the average polarization rotation at the current sample angle. Then the code automatically rotates the sample to the next angle value encoded and, after pausing for ~1/2 a second to allow mechanical vibrations in the setup to dissipate, repeats the measurement. Hence, the procedure is completely automated, and the system can operate autonomously for days without losing stability. Moreover, since the cycling of the magnetic field is repeated at a fast rate, this setup is insensitive to DC noise of non-magnetic origin.

Figure 2.2 shows the user interface for the program – the top left plot displays the driving magnetic field, below it is the magnetization, both plotted against time, and on the right is M vs. H, displaying the hysteresis loop. Note that after amplification and band-pass noise filtering, the signal is strong enough to be easily seen and measured without any averaging, as is done for the trace in figure 2.2. The lines on the hysteresis plot in the figure show some of the measured parameters of the loop. Further, the frequency at which the field can be cycled for the measurement is limited only by the magnet's power supply and the field required to reach saturation. As the frequency increases, the inductive resistance of the coil becomes large, and hence the current and the produced field drop. However, this limitation is fairly loose, and with our setup, we were able to measure hysteresis at rates of up to ~120Hz – the trace in figure 2.2 was taken at 100Hz cycling frequency.

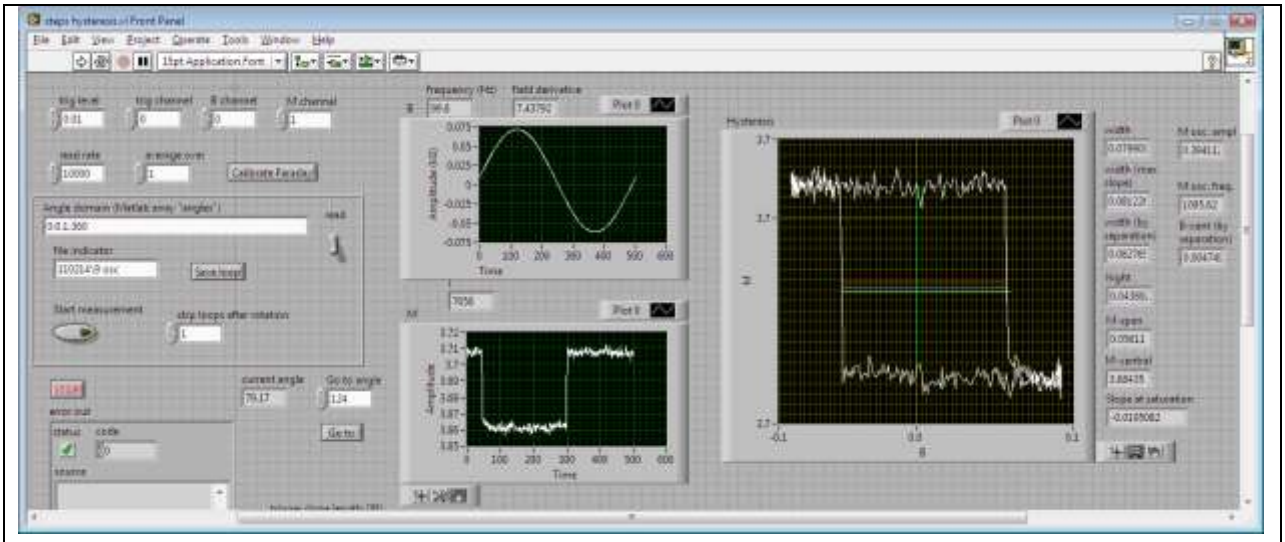

Fig.2.2. Controlling program GUI The traces are: top-left – H vs. time, bottom-left – M vs. time, right – M vs. H. The traces were taken without averaging, at 100Hz field cycling frequency.

2.3 Data and discussion

The above system was used to measure the properties of four different iron-gallium films. The first film studied was 8 nm thick Fe-Ga, with ~15% gallium concentration (see fig. 1.4) grown on an MgO crystal substrate with (100) lattice orientation (see fig.1.4). The lattice mismatch between iron and MgO is 3.5%, with the iron lattice being smaller. The Fe-Ga lattice is slightly larger than that of pure iron (<1% difference), and hence the lattice mismatch for this is somewhat smaller. This mismatch then creates a proportionate strain in the film. The second film considered was 17 nm pure iron, also grown on MgO (100), to be used as a reference. This film turned out to exhibit more complicated hysteresis behavior, and hence we avoid discussing it first. The third film was ~17 nm thick Fe-Ga with 22% Ga concentration, on a Ge substrate, now in (110) orientation. The lattice mismatch between Fe and Ge is 1.4%, with iron being larger, and hence the mismatch for Fe-Ga will be slightly worse. Note that the strain here will be opposite to that in films on MgO. Finally, the fourth film, is exactly the same as the third (same material,

same substrate, was grown simultaneously), but the lattice is in the (100) orientation. Following is the collected data.

Film 1: Fe + 15% Ga on MgO (100)

This sample shows the magnetocrystalline anisotropy effects most clearly, directly following the four-fold geometry of the cubic lattice. First, we present the magnetic anisotropy of the sample by plotting the coercivity field extracted from the measured hysteresis loops (the width of the loop) and the remanence (the height of the loop at zero field) versus the orientation of the sample relative to the applied field (fig.2.3.1, (a) and (b) respectively). A measurement such as this takes about 5-10 minutes with the designed setup, depending on the coercivity saturation fields and is done using 0.1^{o} increments for the sample's azimuthal angular orientation. One intriguing feature of the anisotropy plot from Fig.

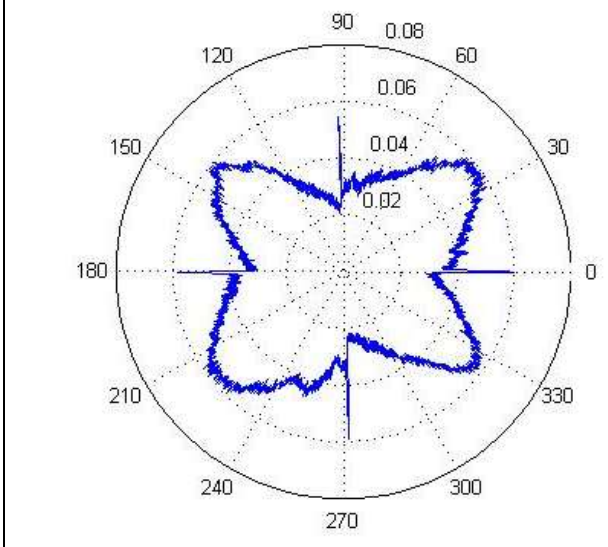

a)

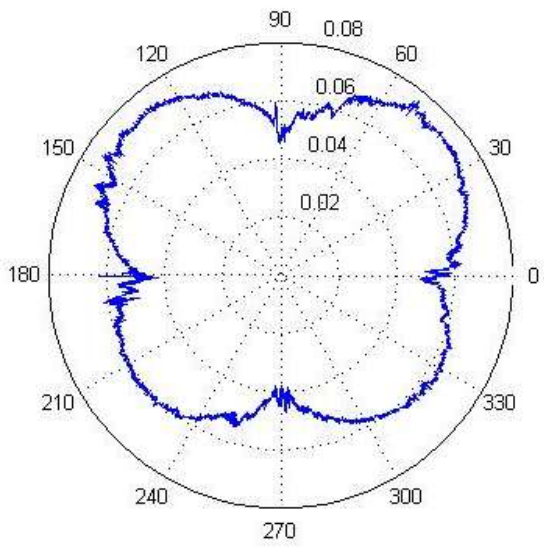

b)

Fig.2.3.1. Magnetic anisotropy (a) coercivity field and (b) remanence magnetization versus angle

2.3.1a is in the presence of sharp spikes in coercivity when the magnetic field is applied along the hard axis (to within ±1^{o} for this sample, but can be much narrower for other samples). Also note that the easy axes of the anisotropy lie along the diagonals of the Fe-Ga lattice here.

To understand these plots better, consider the hysteresis loops at the various angles (fig. 2.3.2). At the easy axis (at 40^{o}), the loop looks very square, as expected from the discussion in section 1.4. Note that the shape of this loop remains essentially unchanged for angles all the way up to a few degrees from the hard axis. Near the hard axis however (around 0^{o}), the loop does not collapse to a line as promised in section 1.4. This is because the discussion in that section focused on samples with uniaxial (two-fold) symmetry, whereas this sample is four-fold.

The exact dynamics of magnetization reversal in this case are not easily measured, and hence are difficult to know for certain. A plausible mechanism that qualitatively yields all the observed results is as follows. Unlike in the uniaxial case, where the mgnitization can rotate uniformly through the easy axis to the other side, here it has to pass through two easy axes, separated by another hard axis. Therefore, after the magnetization rotates to the nearest easy axis, it remains there until the energy disbalance becomes large enough for domain nucleation and wall motion to take place, which is energetically easier than rotation through a hard axis. Then, the magnetization abruptly jumps either to the other easy axis or directly to its final state at the reversed hard axis, depending on the Zeeman vs. MCA energy balance at the time. This sequence of steps then produces the exact loops seen at and near the hard axis (fig.2.3.2). Also, since the exchange energy does not increase as much for a 90^{o} spin adjustment than for a 180^{o} one, the domain walls between orthogonal domains require less energy than those between anti-aligned domains. Hence, domain nucleation and propagation does not require as much energy for a 90^{o} magnetization rotation, which gives the reason for why the loops seen at -2^{o} and 2.5^{o} are narrower. If the magnetization starts at exactly the hard axis however, then unlike the near-

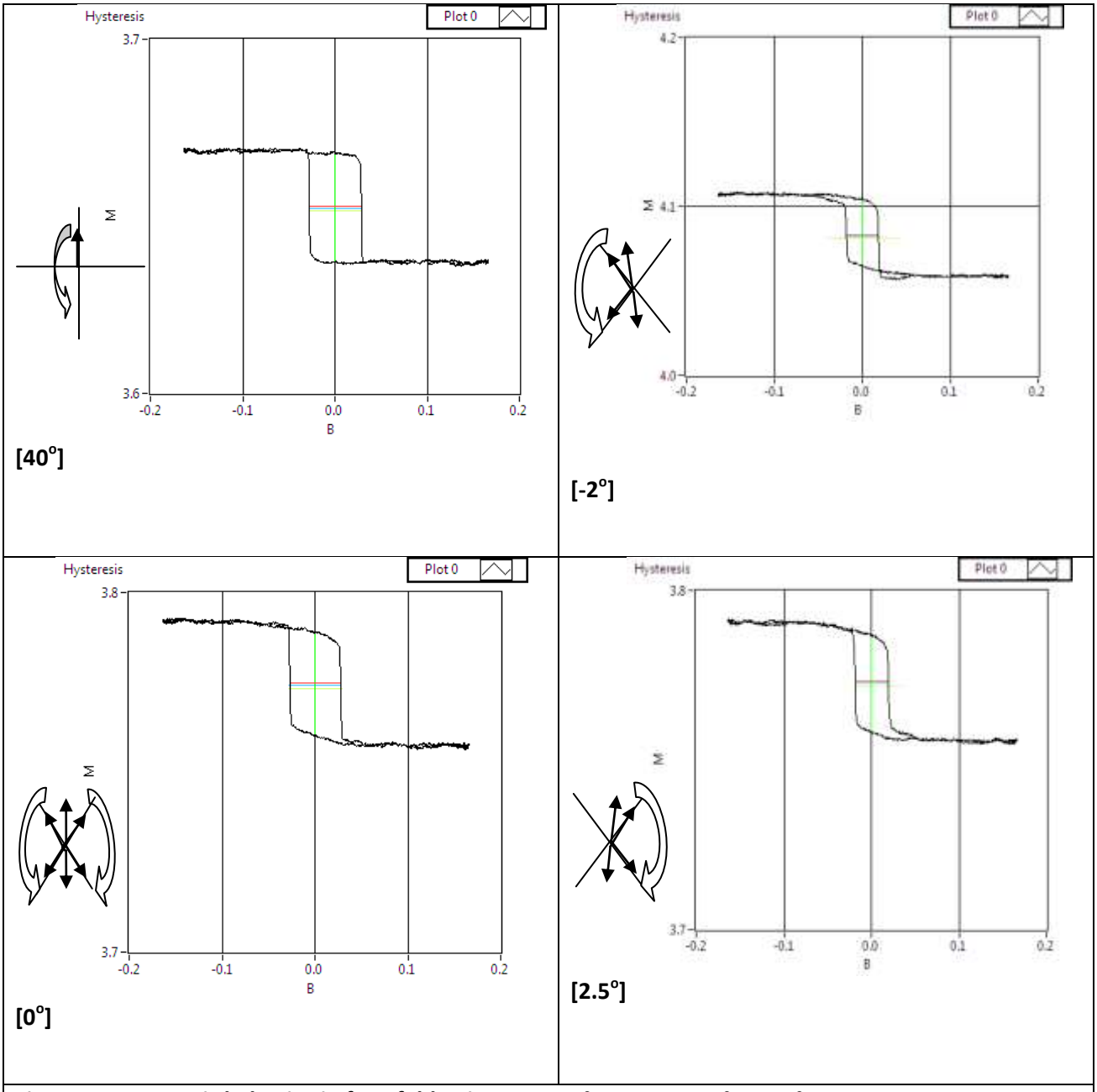

Fig.2.3.2. Hysteresis behavior in four-fold anisotropy (40°) – easy axis, (-2° and 2.5°)- near-hard axis on either side, (0°) – exactly on the hard axis. The diagrams on the left show the mechanics of magntization rotation (axes represent the easy axes)

hard scinareos, the original spin rotation is not uniform. Hence, spins align along both of the adjacent easy axes, which is magnetostatically more favorable than along just one, and hence, more stable.

This mechanism then explains the structure of the plots in figure 2.3.1, including the abrupt spikes at the hard axes. The only piece it is missing is the fact that the coercivity at the easy axis and at

the spike at the hard axis is observed to be the same. This fact is not enforced by the above explanation and would indicate that the energy required for reverse-domain nucleation, less the magnetostatic destabilization is about the same as the energy of orthogonal domain nucleation.

Film 2: Fe on MgO (100)

Despite the seeming simplicity of being a pure material sample, this film exhibited some very strange and interesting behavior. Figure 2.3.3a displays the hysteresis loops as the angle approaches and passes the hard axis of the material (easy axis at 43^{o}, hard at 0^{o}). From this, we can already see that something very unusual is happening. However, double-step hysteresis that might look similar to this is sometimes observed in materials with four-fold anisotropy – we can even see traces of such behavior in figure 2.3.2. What makes this behavior strange, is that the observed steps are not due to linear polarization rotation expected from longitudinal MOKE. This can be shown by varying the angle of the analyzer, as is done in fig.2.3.3c. If the polarization is linearly rotated by the magnetization, then by setting the analyzer angle exactly at extinction, the signal should disappear because the derivative of the transmission function at that angle is zero (see fig.2.1b). Similarly, by rotating the analyzer to the other side of extinction, the signal should reverse sign, because so does the derivative of the transmission function. This behavior is indeed observed in most cases, such as for the easy-axis hysteresis loop here. However, while the loop reverses sign upon passing extinction by the analyzer, the steps do not, as can be seen in fig.2.3.3c. They are also the only signal not eliminated by setting the analyzer to extinction, and hence, their behavior can be studied in isolation as shown in fig.2.3.3b. This behavior is very different from anything else observed in these studies – particularly intriguing is the appearing hysteresis curve that reverses orientation with angle. This reversal is very sensitive to the angle, and has

been observed to have some metastable character. Note that these loops are many times smaller than those typically measured – the displayed plots required averaging over 300 traces to filter the noise.

Such behavior indicates that these signals are either extra elliptically polarized components created upon interaction with the film, or changes in reflectivity of the entire signal. This can be tested by placing a $\lambda/4$ waveplate in from of the analyzer. If the steps are due to elliptically polarized components, then when the waveplate is aligned with the long axis of the ellipse, the polarization will become linear upon passing through, and can then be blocked by a correct analyzer orientation. If we assume that the ellipse's long axis is aligned with the polarization of the incident beam, then we know that the correct orientation of the waveplate will not affect any of the linearly polarized components. Hence we can align it by assuring that at extinction the waveplate does not affect the signal. When this is done, and the analyzer is subsequently rotated, we obtain the plots in fig.2.3.3d. The second of these shows extinction of the step components, while the other plots show their reversal, as predicted by ellipticity hypothesis. This could, of course, not be possible if the steps were a result of a reflectivity change.

a)

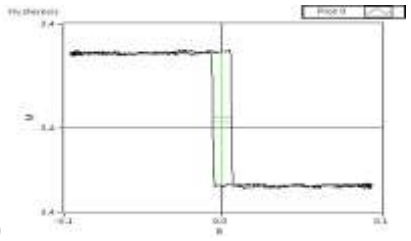

43 °)

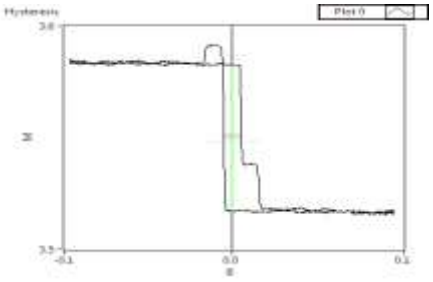

-7 °)

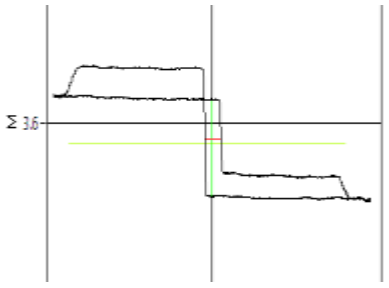

-2 °)

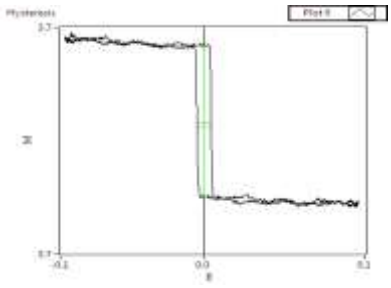

0 °)

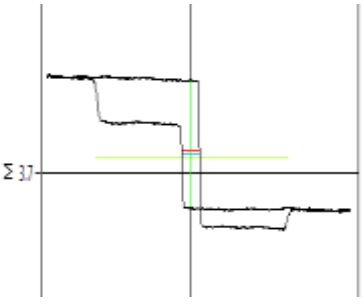

2 °)

b)

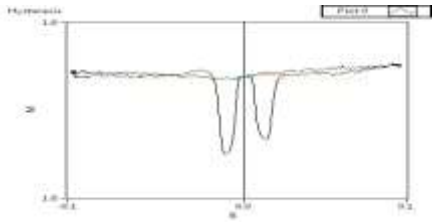

11.3 °)

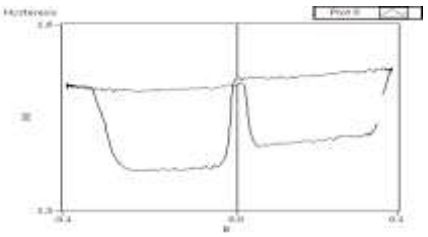

3 °)

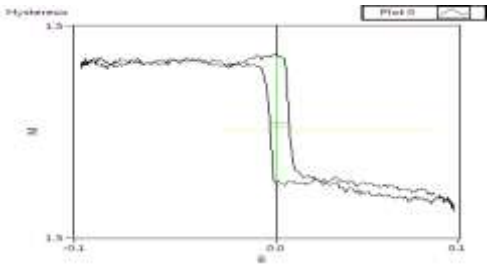

2.8 °)

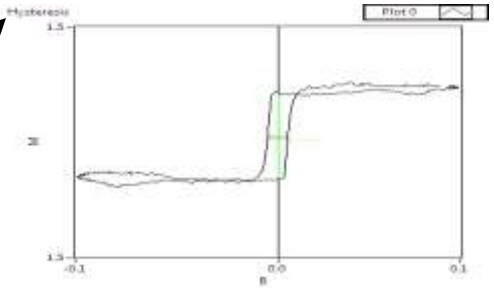

0 °)

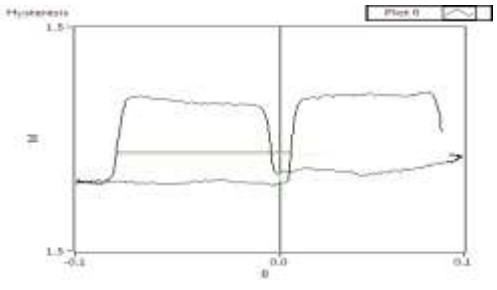

-0.5 °)

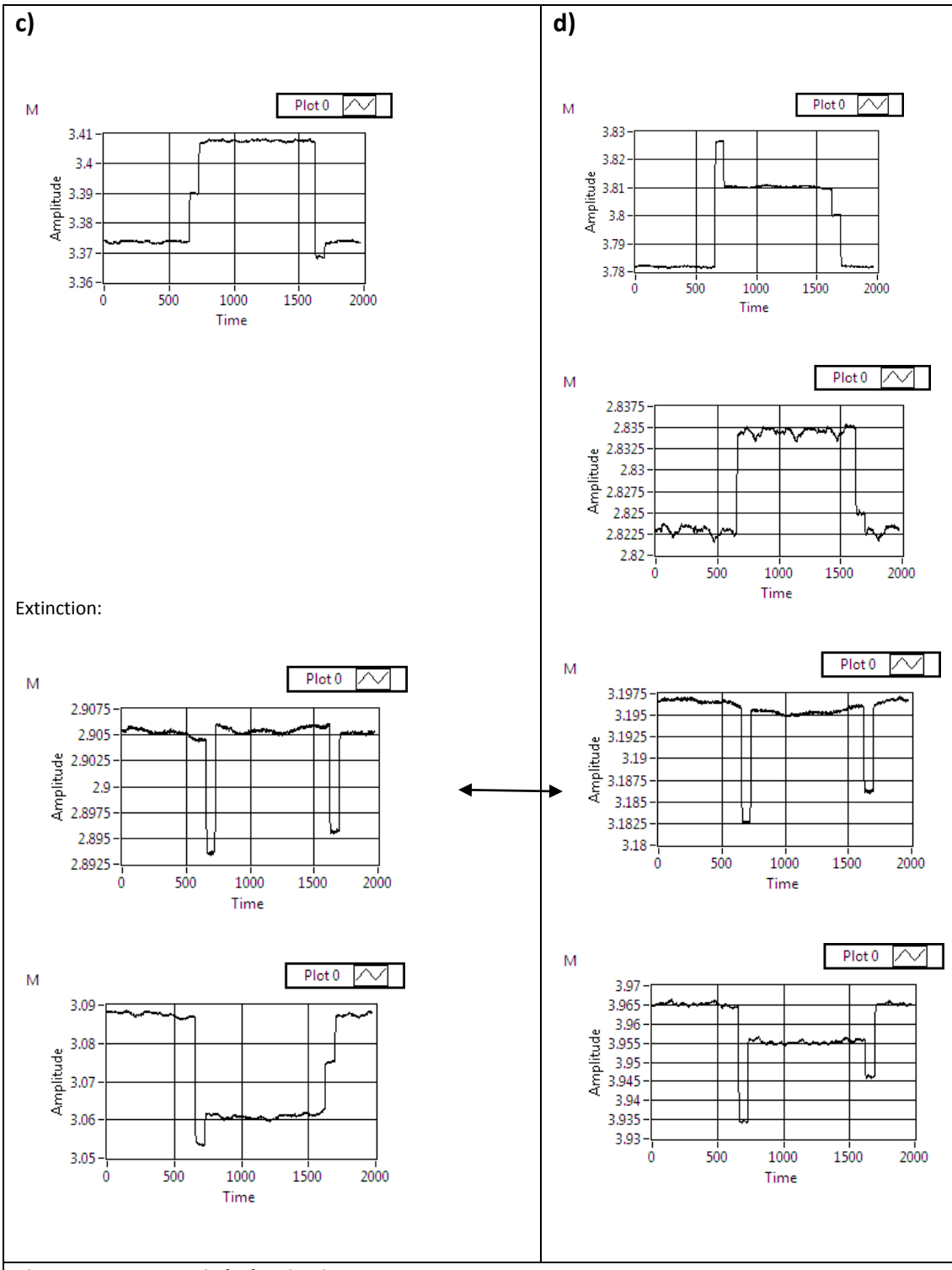

Fig.2.3.3. Hysteresis behavior in Iron (a) – a sequence of hysteresis loops measured passing the hard axis; (b) – a similar sequence, but with analyzer set at extinction; (c) – the magnetization signal at different analyzer angles; (d) – the magnetization signal for different analyzer angles with an added λ/4 waveplate.

All above considerations lead us to believe that these steps are caused by the non-longitudinal components of the magnetization. This could be possible either through second-order MOKE, which depends on the product of the different magnetization components, or through a non-zero polar component of the magnetization. Furthermore, we can look at the magnetic anisotropy by studying the plots of the coercivity, remanence and of the field required to overcome the steps (the step width) against angle (fig.2.3.4). At first, the coercivity does not seem to change much; however, although the slight variations in it seem to be noise-like, the pattern is reproducible for the given sample. The plot of the step width, on the other hand, seems to indicate that there is some enormous anisotropy in the sample, even if it does not show up in coercivity. This is also not true, because as the angle approaches a hard axis, the steps seem to become wider and shorter asymptotically. Thus, the height of the spikes in fig.2.3.4b does not have any physical meaning, and is simply determined by the signal to noise ratio and resolution. The remanence plot on the other hand clearly displays the familiar four-fold anisotropy of the iron lattice.

From the data collected, the exact origin of the observed additional elliptically polarized component is not clear. It seems most likely that it comes from other magnetization components that appear from uniform spin rotation in the course of magnetization reversal process. This would also explain why the steps disappear if the magnetization is originally oriented exactly along the hard axis (in that case, the spin rotation is not uniform, and hence the contributions cancel). For example if the reversal pathway involves domain rotation to some stable orientation near the spike position, with a component normal to the film surface (if the increase in the magnetostatic energy is somehow balanced by other factors), then the polar MOKE would occur along with the longitudinal one, and the two could produce an elliptical polarization. This possibility is especially worth considering since the polar MOKE in iron is generally ~6 times stronger than longitudinal. However, to be able to conclusively state the reversal

pathway and to determine the cause for the observed steps, other techniques and measurements are necessary, some of which could be done with further development of the system built here.

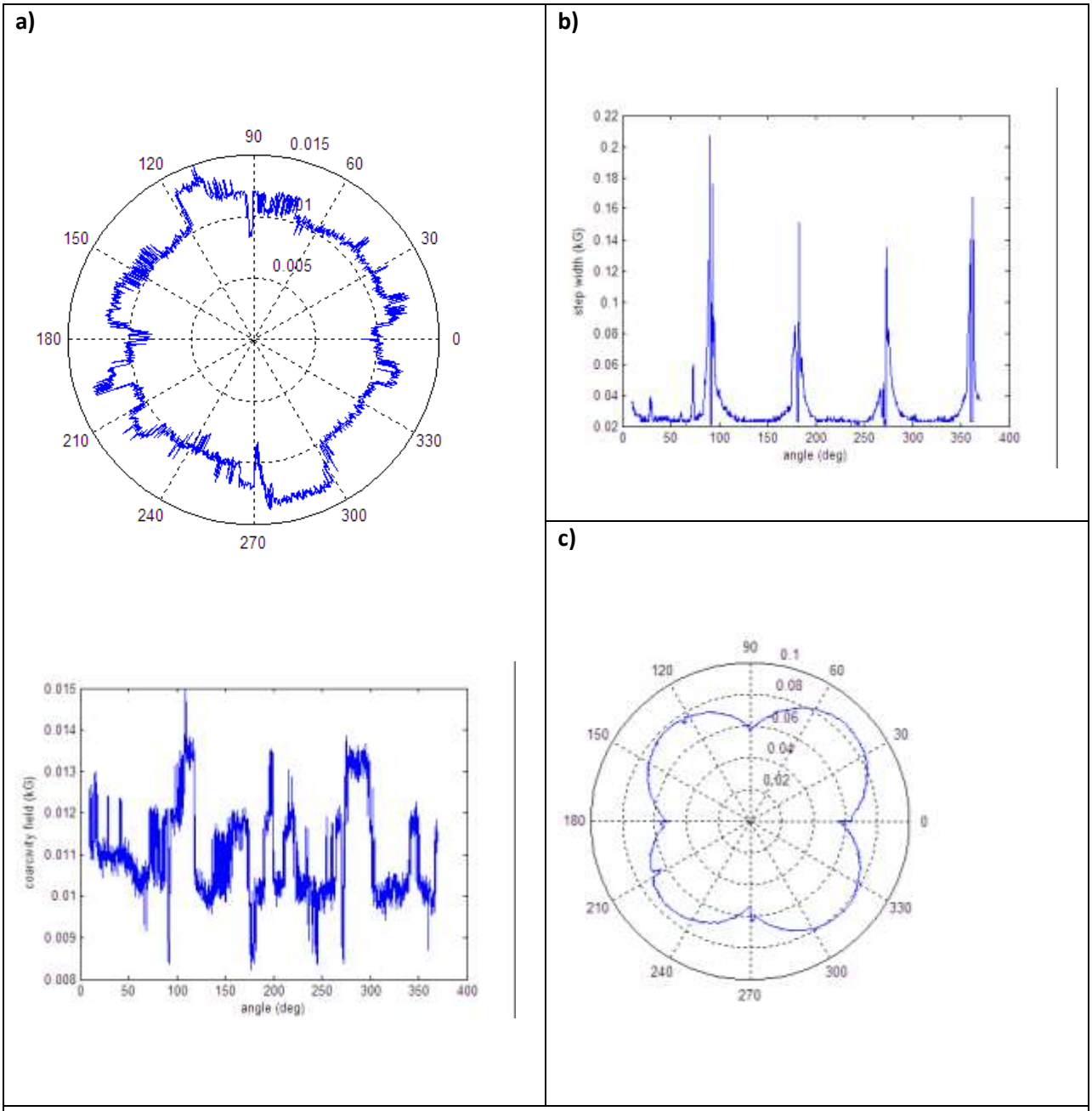

Fig.2.3.4. Anisotropy in Iron (a) – coercivity field vs. angle (polar and Cartesian plots), (b) – field required to overcome the observed step and completely saturate the sample vs. angle (Cartesian), (c) – remanence magnetization (polar)

Film 3: Fe + 22% Ga on Ge (110)

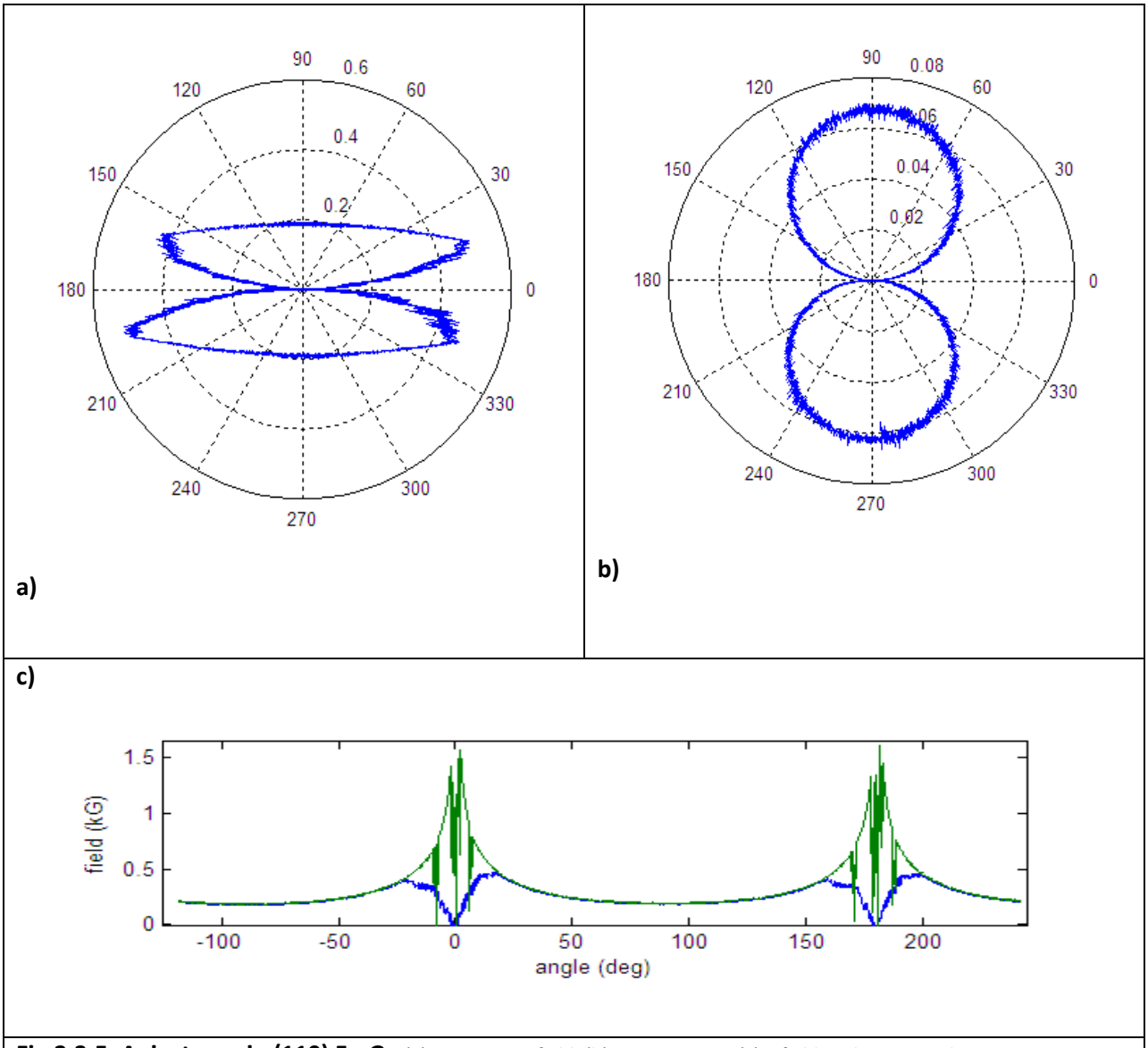

Fig.2.3.5. Anisotropy in (110) Fe-Ga (a) – coercivity field, (b) – remanence, (c) – field to domain nucleation

The FeGa sample grown on (110) Ge substrate shows a very nice uniaxial sample that followed the predictions of section 1.4 almost exactly. Figure 2.3.5 displays the coercivity and remanence anisotropy measured, while figure 2.3.6 shows the loop shapes at various angles. The easy axis loop at 90^{o} is very square, as predicted, while the hard-axis loop at 4^{o} is very nearly just a line (the small discrepancy is due to sample imperfections and measurement error) (see figure 1.3). The only point that remains to consider here is the reversal dynamics when magnetization is starting from a near-hard axis. In that case, the spins first rotate uniformly to the easy axis, and pass it. In order to get to their final reverse state, they would then have to pass over the other hard axis. However, as they approach the hard axis, the MCA energy increases, and eventually becomes enough so that domain nucleation is preferable to further motion towards the hard axis. Hence, at the point, the magnetization rapidly

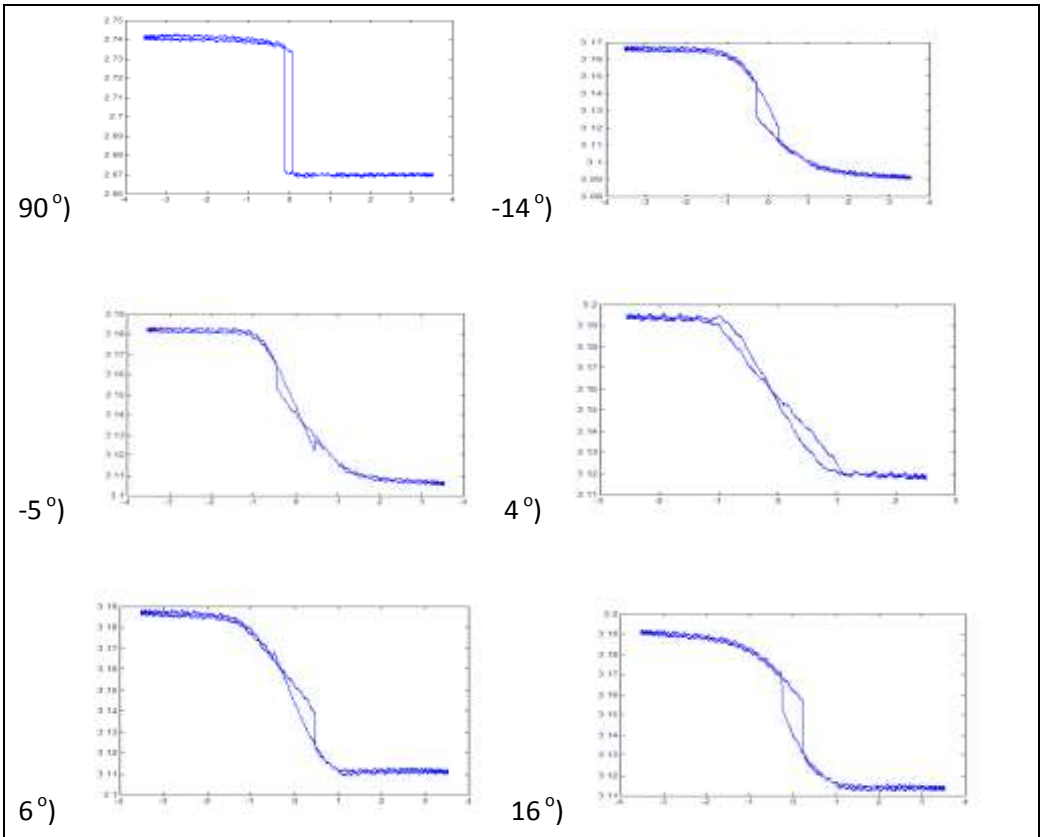

Fig.2.3.6. Loops passing through hard axis for (110) Fe-Ga

changes to its final state via domain wall motion mechanism. This is then the origin for the observed abrupt jumps in the near-hard loops. Note that in some cases, it is easier to nucleate domains starting from the easy axis, and hence it could become energetically favorable for the magnetization to rotate slightly against the applied field before the transition (fig.2.3.6, -5 ^{o}).

One other aspect that is interesting to consider is the magnetic field required for the abrupt transition for the final state to occur. This, in a way, allows measuring how "hard" the hard axis is. To see this, we look at the magnetic field between the two points on the loop with the maximum derivative. The result is plotted in figure 2.3.5c along with the coercivity. The curves overlap perfectly everywhere except near the hard axis for obvious reasons.

Film 4: Fe + 22% Ga on Ge (100)

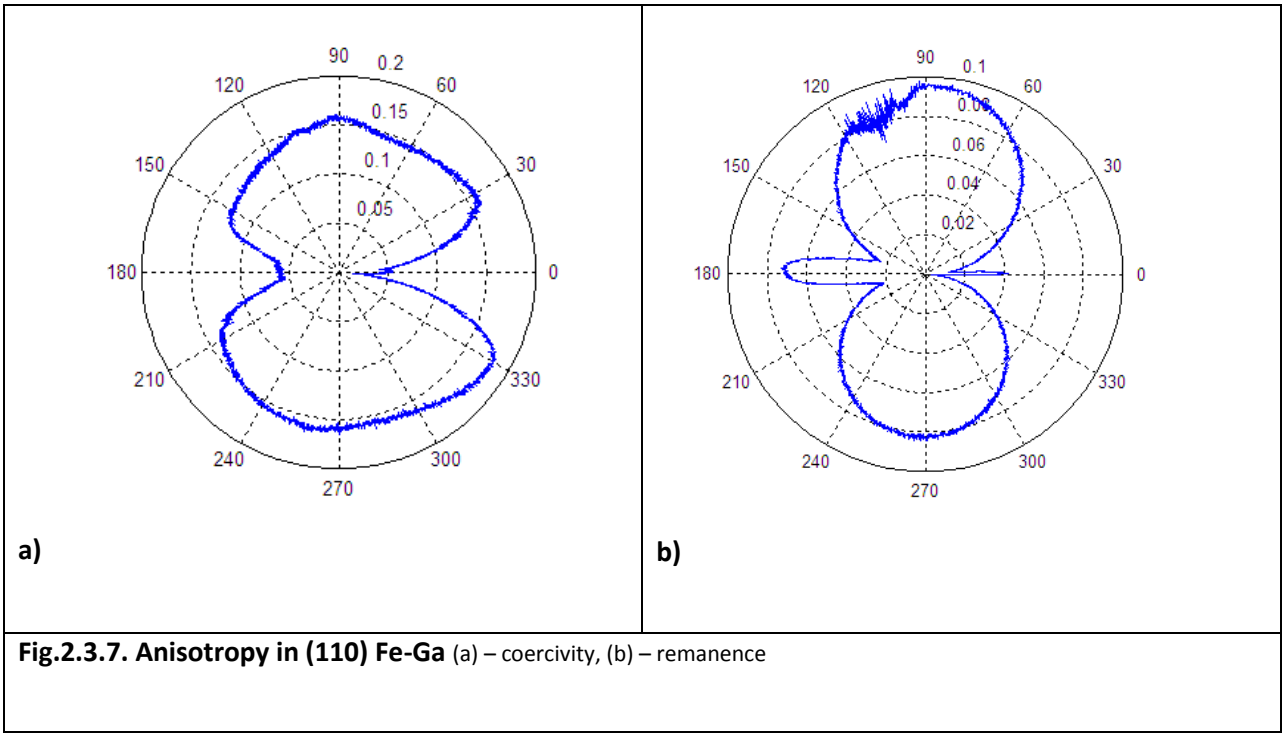

Fig.2.3.7. Anisotropy in (110) Fe-Ga (a) – coercivity, (b) – remanence

The FeGa sample grown on (100) Ge substrate also shows interesting behavior. Although the substrate lattice for this sample has a (100) orientation, thus promoting (100) orientation for the film, its anisotropy seems to be a curious mixture between the uniaxial and fourfold (fig.2.3.7). This is most clearly seen on the remanence plot, but can also be anticipated from other plots and from the loop shapes (fig.2.3.8). In particular, the loop at the hard axis is clearly different from that observed for the hard axis of the (110) lattice above. The main difference is that here, the loop encloses a non-zero area, and thus follows some of the dynamics discussed for the case of film 1. Most of the other loops for this sample look very similar to those for film 3, as can be seen in figure 2.3.8. The reason for the near-uniaxial symmetry of this sample could be in some other source of anisotropy that dominates over the MCA, such as if there is a large strain in the film along one direction. Another possible explanation could be in that the film lattice does not follow the (100) orientation promoted by the substrate exactly, and actually has some midway orientation.

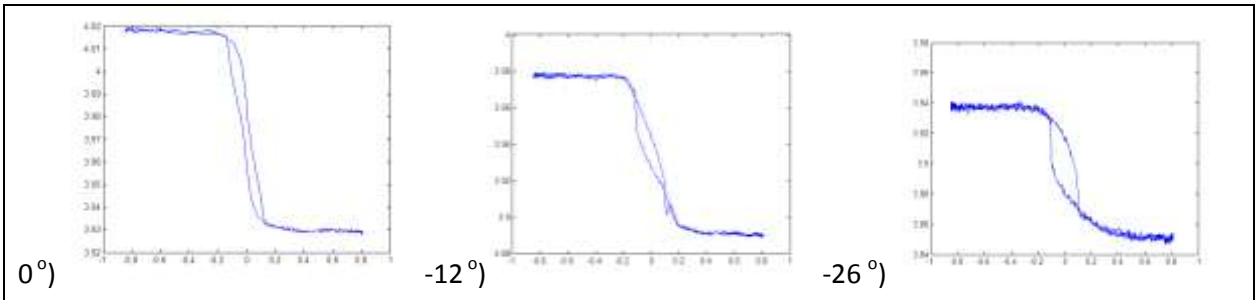

0 ^{o}) -12 ^{o}) -26 ^{o})

Fig.2.3.8. Loops near hard axis for (100) Fe-Ga

3. Spin-wave measurements

The second part of this work was the measurement of spin waves excited in a film by a perturbing laser pulse and measured via the time-resolved Magneto-Optical Kerr Effect (TR-MOKE) in a pump-probe setup that is using femtosecond pulsed lasers. This method can also be used to measure the sample magnetic anisotropy, as well as several other important magnetic parameters. The main difference between this measurement and that of hysteresis is that the hysteresis method looks at the overall behavior of the film during complete magnetization reversal and saturation, while TR-MOKE measurement senses very small dynamical perturbations of the magnetic structure of the film as well as the relaxation on short time scales. These TR-MOKE measurements were then performed on the same four Fe-Ga samples as the hysteresis measurements in Chapter 2.

3.1 Experimental method

The experimental setup used for TR-MOKE measurement is shown in figure 3.1a. As can be seen, the experiment here is quite a bit more complicated than the one for hysteresis measurement. This is because the time resolution required to detect spin-waves is ~ picosecond, and hence direct measurement is not possible due to detector limitations (which in our case has the resolution of ~70ns). Hence, a pump-probe setup is implemented, in which 150 fs probe laser pulses at 100MHz repetition are used to detect the MOKE, thus only detecting the magnetization within the 150 fs time frame and allowing the desired resolution. Then, in order to match the slower time resolution of the detector, the laser pulses must measure the same magnetization value throughout the 70 ns detector time step. The only way to ensure that the spins will have the same orientation for every probe-pulse measurement is to enforce some specific initial conditions shortly before the probe pulse. Thus, a stronger pump laser

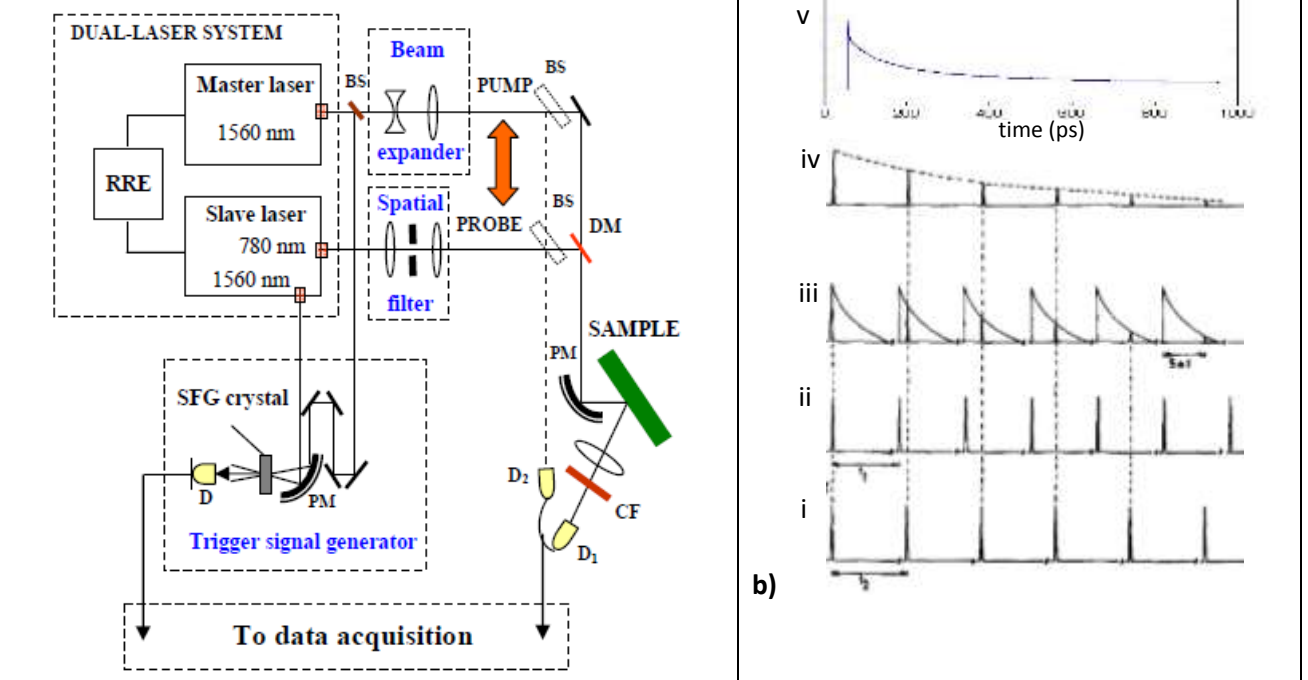

Fig.3.1. Experimental setup (a) – the experimental pump-probe setup [12], (b) – mechanism of automatic probe delay scanning via pulse train frequency difference [13]

pulse is incident on the sample at a fixed time before the probe, perturbing the spin orientations within the 3 μm diameter focal spot by coupling thermal energy to strain to magnetization. As the resulting spin-wave relaxes, it does not propagate due to the dispersion relation, and so the spins all precess in phase. Hence, a probe pulse incident at a fixed time after the pump will detect the same magnetization each time, allowing to measure it with 150 fs time resolution.

Then, to measure the magnetization precession and spin-wave relaxation time dependency, the delay between the pump and the probe pulses needs to be adjusted. This can be done automatically by setting the frequencies of the pump and probe to slightly different values, thus producing a gradual phase shifting between the two. Figure 3.1b illustrates this mechanism – plots i) and ii) show the probe and pump pulse trains respectively, plot iii), the spin wave relaxation after the pump with the indicated

positions measured by the probe each time, plot iv) shows the resulting measured signal, and plot v) displays the data from a real measurement. From this, we see that above 150 fs, the difference in frequencies between the pump and probe pulse trains will determine the temporal step of scanning as well as the time resolution and also the scanning speed of the measurement.

3.2 Experimental setup

The experimental setup in fig.3.1 begins with the two lasers systems that are locked in by a feedback loop to operate with a fixed frequency difference (~ 1 kHz), and at 100 MHz repetition rate. Small portions of the two pulses are picked off and focused together onto a Sum Frequency Generation (SFG) crystal, where double absorption and hence second harmonic generation occurs only when the two pulses are temporally overlapped. The second harmonic signal is then used to trigger the data acquisition for recording the scan on a PC.

The remaining portion of the probe laser is frequency doubled, which then allows using a dichroic mirror to send the pump and the probe along the same path to the sample. The two pulses are then focused onto the sample to provide a high enough intensity for excitation. Focusing is done by a parabolic mirror to avoid chromatic aberrations, and produces a 3 μm diameter focal spot for the pump, with half-size probe spot due to the wavelength difference. Finally, after reflection, the pump signal is filtered out by an interference filter, and the probe goes to the detector. If the polarization rotation is measured, then the beam also passes through an analyzer. To additionally allow measuring reflectivity variations, the detector is balanced by another signal of equal unperturbed intensity that is split off from the probe before it interacts with the sample. This allows the detector to cancel the unwanted DC background during the reflectivity measurement. These reflectivity measurements can then be used to

detect phonons and strain in the sample and provide also with the experimental rate of sample cooling following the pump pulse excitation [12].

3.3 Results and analysis

The above setup was then used to measure the spin-waves in the same four samples that were measured in chapter 2 (see section 2.3 for details). For each sample, the waves were measured using the polar MOKE configuration, with a constant external magnetic field of 0.8 kG applied along the easy and the hard axes (two traces for each sample). Note that due to the symmetry of the spin potential around the easy and the hard axes, if magnetization is oriented exactly along either axis, the perturbing pump pulse will only adjust the magnetic potential well vertically, without affecting the spin orientations. Hence, the field was applied at 5^{o} from the easy and the hard axis in each case.

Figure 3.2 then illustrates the obtained results. In each plot, the top trace was taken when the external field, and hence magnetization, was oriented along the easy axis, and the bottom – for M along the hard axis. In these plots, the slowly varying background is due to a change in reflectivity and is unrelated with the magnetization. Hence, the only properties of these traces we are interested in are the frequency, amplitude and the decay time. The oscillation frequency and amplitude both depend on the shape of the potential well in which the spins are confined to precess, and hence on the structure of the potentials near the easy and the hard axes. Generally, since the well at the easy axis is formed by the combined effect of the MCA and the Zeeman energies, it is sharper, deeper and narrower than the well at the hard axis, where MCA acts to flatten out the Zeeman potential. This should then result in lower-amplitude and higher frequency oscillations at the easy axis for the same perturbing energy. This is clearly supported by the plots for films 2 and 3. The two frequencies and amplitudes for films 1 and 4 on the other hand, are identical to within the error, indicating similar potentials at the easy and the hard

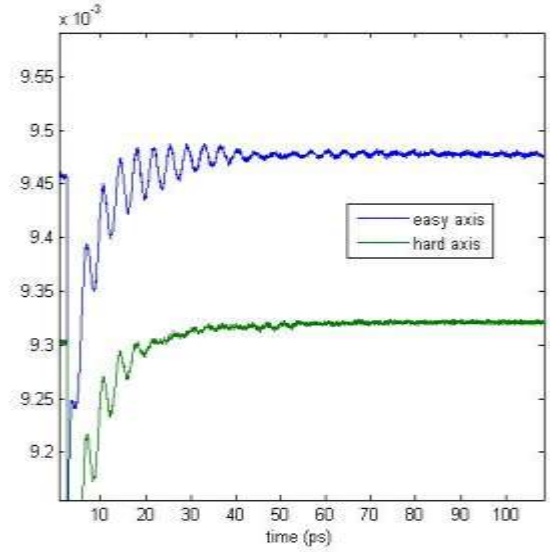

Film 1: Fe + 15% Ga on MgO (100)

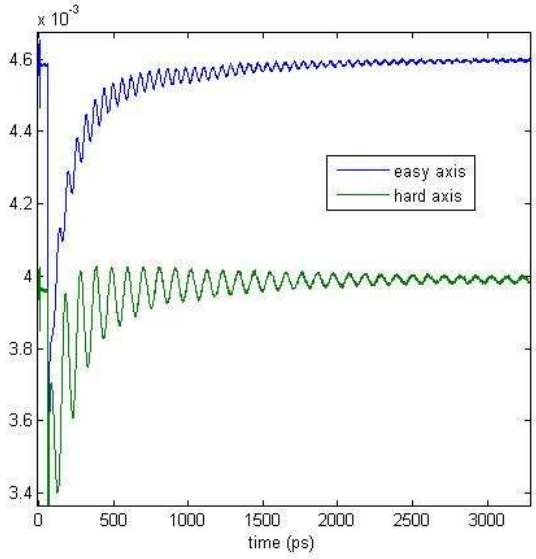

Film 2: Fe on MgO (100)

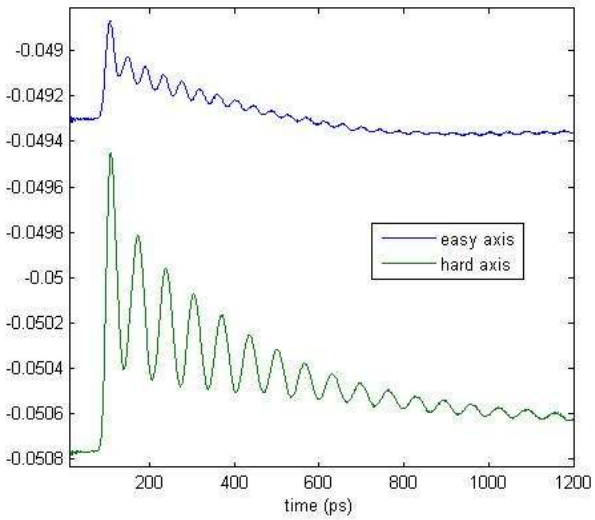

Film 3: Fe + 22% Ga on Ge (110)

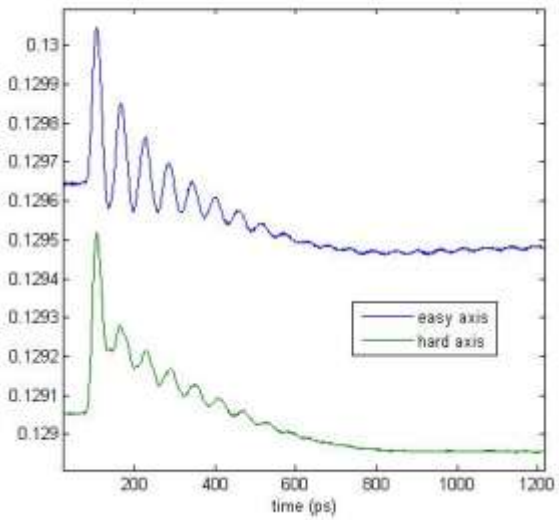

Film 4: Fe + 22% Ga on Ge (100)

Fig.3.2. Spin-waves: the spin waves measured for the four samples. Top trace- magnetic field applied along easy axis, bottom trace – along hard axis in all plots. Slowly varying background is irrelevant.

axes, and hence, smaller anisotropy. Recall that samples 2 and 3 did exhibit more dramatic anisotropic behaviors in the hysteresis measurements as well.

Finally, the decay time scales are related to the coupling between the magnons and the phonons, and hence depend on the magnetoelastic coupling coefficients in the material. Thus, the observation that the decay time is independent of magnetization orientation, which can be made based on the plots, is expected. Note that decay time is shorter, and hence magnetoelastic coupling is stronger, in films 1 and 4 – where anisotropy is weaker. This is, of course, not enough evidence to correlate the two phenomena, but a few reasons could be argued for why this should be true. As we can see, since we only have three parameters to work with in these plots, it is difficult to obtain much qualitative information from them – precise modeling and calculations are required to obtain most useful information here. The last interesting thing to note is that in the easy-axis trace for film 1 in particular, a slight beating behavior may be observed. This can also be seen upon more careful examination of the other plots, and could indicate several slightly different normal modes for the spin precession that are excited.

4. Conclusion

In this work, we demonstrated the capability of hysteresis and spin wave magnetometry applied for epitaxial FeGa samples. These samples are of high interest due to their application potential related to the very large magnetostriction characteristic for FeGa. We observed that the magnetic properties of epitaxial FeGa films are very strongly dependent on the substrate choice or its orientation. The hysteresis magnetic loop tracer was developed and optimized to provide state of the art performance:

high stability, high sensitivity and short data acquisition times. Hysteresis studies allow significant insight into the dynamics of magnetization changes in thin films, and the improved setup developed here has already allowed for new measurements that would previously have been very difficult. The data collected with a pump-probe laser setup have provided to be very useful for probing the real time spin dynamics in FeGa. This opens the possibility to study the correlation between the laser generated strain in FeGa and the properties of spin waves in the large magnetostriction material.

Following this work, the two systems will be combined into one to allow both measurements to be performed simultaneously, and hence under identical conditions. This will allow isolating some parameters and dynamics that are otherwise inseparable from other factors. Additionally, we plan to adjust the hysteresis setup to allow spatially resolved magnetization measurements, and hence direct visual observation of domain wall propagation and magnetization reversal dynamics in thin films. The understanding of the mechanisms governing magnetization then has many immediate practical applications, including novel methods of electronic information storage, sensing, micro-manipulation in nanotechnologies and many others.

Acknowledgement:

We thank Yves Idzerda [11] for providing the Ge-substrate samples that were used in this work.

References

1. Elizabeth R. Smith, “Probing the Magnetic Anisotropy of Co/Cu Thin Films,” U of M PhD thesis, 1998

2. R.F. Soohoo, “Magnetic Thin Films,” Harper & Row, 1965
3. C. Kittel, “Introduction to Solid State Physics,” John Wiley & Sons, Inc., 7ed., 1996
4. Domain wall picture from <http://dpmc.unige.ch/gr_giamarchi/research.htm>
5. Domain photograph from <http://en.wikipedia.org/wiki/Magnetic_domain>
6. Hysteresis schematic from <http://en.wikipedia.org/wiki/Hysteresis>
7. [1] and R.A. Lukaszew, Z.D. Zhang, V. Stoica, R. Clarke, “Characteristics of Ni films deposited on SiO2/Si(1 0 0) and MgO(0 0 1) by direct current magnetron sputtering system with the oblique target,” Appl. Surf. Sci. 219, 74 (2003).
8. MOKE components diagram from <http://en.wikipedia.org/wiki/Magneto-optic_Kerr_effect>
9. J. M. Florczak and E Dan Dahlberg, “Detecting two magnetization components by the magneto optical Kerr effect,” J. Appl. Phys. **67** (12), 15 June 1990
10. Bader, S. D.; Parkin, S. S. P., “Spintronics,” Annual Review of Condensed Matter Physics, vol. **1**, p.71-88
11. Adam McClure,a_ H. Li, and Y. U. Idzerda, “Magnetostrictive effect in single crystal Fe1−xGax thin films,” JOURNAL OF APPLIED PHYSICS **107**, 09A924 _2010
12. Spin waves, and picture: Vladimir A. Stoica,* Yu-Miin Sheu, David A. Reis, and Roy Clarke, “Wideband detection of transient solid-state dynamics using ultrafast fiber lasers and asynchronous optical sampling”
13. E. Lill, S. Schneider, and F. D6rr, “Rapid Optical Sampling of Relaxation-Phenomena Employing Two Time-Correlated Picosecond Pulsetrains, ” Appl. Phys. **14**, 399-401 (1977)